Desalination and Water Treatment
www.deswater.com
doi: 10.1080/19443994.2015.1035675

57 (2016) 8854–8862
April

Taylor & Francis
Taylor & Francis Group

Photochemical degradation of methylene blue by metal oxide-supported activated carbon photocatalyst

A. Nasrollahpour, S.E. Moradi*

Young Researchers and Elite Club, Islamic Azad University, Sari Branch, Sari, 48164–194, Iran, Fax: +98 11 33363168; email: er_moradi@hotmail.com (S.E. Moradi)

Received 4 August 2014; Accepted 1 March 2015

ABSTRACT

Activated carbon photocatalyst with high surface area has been synthesized and modified with iron oxide nanoparticles by microwave heating technique. The surface-modified microporous activated carbons were characterized by BET surface area and XRD analysis. Degradation experiments were conducted in batch mode with the variables such as contact time (0–120 min), photocatalyst dosage (0.01–0.2 g/L), initial solution concentration (50–150 mg/L), and solution pH (2–10). The iron oxide-modified activated carbon (3-Fe-MAC) was found to be more active compared to the free iron oxide nanoparticles and pristine activated carbon for methylene blue (MB) degradation. Kinetic studies on the photocatalytic degradation of MB using zeros, linear regression data suggested that the degradation followed first-order kinetics. The optimal conditions for the degradation of MB dye were 75 min, 100 ppm dye concentration, neutral pH, and 0.13 mg/L of 3-Fe-MAC dosage.

Keywords: Activated carbon; Iron oxide nanoparticles; Microwave modification; Surface modification; Photodegradation; Methylene blue

1. Introduction

Wastewaters from productions like textile, dying, printing, greasepaints, and food coloring are the main providers of colored wastes [1]. There are more than 100,000 commercially available dyes with over 7×10^5 tons of dyes manufactured by the year [2]. It is expected that 2% of dyes manufactured yearly are discharged in waste from manufacturing operations, while 10% was discharged from textile and associated productions [3]. Discharging of dyes into water resources even in a low quantity can disturb the aquatic life and food web. Dyes can also cause allergic dermatitis and skin irritation. Some of them have been reported to be cancer causing and mutagenic for aquatic organisms and humans [4–6]. Methylene blue (MB) ($C_{16}H_{18}N_3SCl{\cdot}3H_2O$) is one of the most applied dyes [7], it is significant basic dye extensively used for printing calico, cotton, and tannin, indicating oxidation–reduction, and dyeing leather. In purified zinc-free form, it is used as an antiseptic and for other medicinal purposes [8].

Beside adsorption method [9–18], photochemical procedures containing the transition metal ions, mainly iron have attracted significant consideration for degradation of dyes [19–25]. Apart from its benefits such as non-toxic nature, low-cost, and high reactivity, nanostructured metal oxides possess high

*Corresponding author.

band energy and Lewis acid nature which have been exploited for variety of applications such as sensors [26,27], drug delivery [28], and catalyst [29] also it can be extended for photodegradation of dyes [19–25].

To progress its stability and reusability, iron oxide nanoparticles have been immobilized on colloidal solutions, porous glasses, polymers, and alumina. In this context, porous materials with uniform pore sizes, such as activated carbon and activated carbon might, serve as host media for metal oxide nanoparticles. Microwave energy has been used more and more on synthetic organic chemistry because of its great ability to accelerate reactions and to improve yields and selectivity [30]. In recent years, some researchers have started to modify activated carbon samples by microwave irradiation [30].

A detailed survey of literature reveals no information on photocatalytic degradation by iron oxide-supported activated carbon. The iron oxide-supported activated carbon is expected to incorporate the catalytic properties of iron oxide as well as activated carbon apart from high surface area, thermal stability, and chemical inertness of activated carbon. In this study, the effect of microwave modification of activated carbon by iron oxide nanoparticles on MB dye degradation is examined.

This work aims to synthesize and characterize novel microporous activated carbon with high surface area from grapevine rhytidome as an abundant and low-cost precursor via H_3PO_4 chemical activation under microwave, after that additional microwave modification has been done using $Fe(NO_3)_3{\cdot}9H_2O$. The activity of this catalyst was compared with pure iron oxide nanoparticle in the photodegradation of MB in aqueous solution. The effects of contact time, initial solution concentration, and solution pH on MB dye degradation have been investigated. The kinetics analysis and modeling of MB removal via adsorption and photodegradation were carried out.

2. Experimental section

2.1. Materials

The reactants used in this study were the grapevine rhytidome was collected from Sari city's agricultural province and washed several times with distilled water and derived in an oven at 70˚C overnight. The dried materials were crushed to small pieces. Phosphoric acid (85 wt%, Merck Co.) as an activating agent and $Fe(NO_3)_3{\cdot}9H_2O$ (99 wt%, Merck Co.) as functionalization agent, magnetic iron oxide nanoparticles (Fe_3O_4, 99 wt%, Merck Co.), and MB were used.

2.2. Photocatalyst preparation

2.2.1. Microporous activated carbon samples

The novel activated carbon was prepared according to the procedure reported by Hejazifar et al. [31]. In optimum condition, the grapevine rhytidome was added to phosphoric acid with 85 wt% concentration and acid/precursor weight ratio (5:1) for 24 at room temperature. The impregnated samples were heated in a microwave oven (LG, WD700, 2,450 MHZ) with microwave power 400 W, microwave radiation time 2 min. Then the samples were placed in an oven at 110˚C for 24 h. The obtained samples were washed for several times with hot and then cold distilled water to the pH of 7, and dried in an oven at 50˚C overnight. Finally, resultant activated carbons were crushed and sieved to particle mesh size of 20 and stored in a desiccator.

2.2.2. Iron oxide-supported samples

The experimental procedure was carried out using $Fe(NO_3)_3{\cdot}9H_2O$ with prepared activated carbon, and the composition ratio 5.4 gr activated carbon, 2.5 gr of $Fe(NO_3)_3{\cdot}9H_2O$, and 5 gr water has been used. The mixtures were then heated under microwave irradiation (LG, WD700, 2,450 MHZ) by microwave power 400 W for 1–5 min (1-Fe-MAC to 5-Fe-MAC). Nanostructured carbon impregnated with the acetone solution was then filtered and dried at 60˚C for 4 h. The activation temperature was 760˚C and optimum N_2 gas flow rates (250 cc/min) for 2 h were used [32].

2.3. Textural and structural studies

The porous structure of the surface-modified samples was estimated by powder XRD (Philips 1830 diffractometer) using graphite monoarsenated Cu Kα radiation. Adsorption isotherms of the activated carbon samples were obtained using a N_2 gas microporosimeter (micromeritics model ASAP 2010 sorptometer) at 77 K. Pore size distribution and specific surface area were calculated by Dollimore and Heal [33] and BET [34] methods. Pore volume was estimated from the amount of adsorbed N_2 gas at 0.963 in relative pressure, which derives from 25 nm radii pores. Micropore volume was calculated by *t*-plot. SEM images were obtained with JEOL 6300F SEM. Thermal analysis was carried out using NETZSCH STA449C analyzer. The instrument settings were: heating rate 10˚C/min and air atmosphere with 100 mL/min flow rate. For each measurement, about 25 mg of a ground adsorbent sample was used. From

the weight loss curve, the differential weight loss was calculated where peaks represent the weight loss.

2.4. Photocatalytic activity measurements

The photodegradation of MB was done in order to calculate the photocatalytic activity of 3-Fe-MAC photocatalyst. About 10-mg catalyst was mixed with 50 ml of MB aqueous solution (100 ppm) under magnetic stirring in dark for 30 min to reach the adsorption equilibrium of the dye on the catalyst prior to irradiation. The photocatalytic activity of 3-Fe-MAC was evaluated in the degradation of MB aqueous solution under UV irradiation. The UV source was a 125 W Hg lamp with maximum emission at approximately 365 nm. The lamp was placed in an inner irradiation cell in the center of a cylindrical flask (capacity ca. 100 ml) as the reaction vessel. After irradiation and separation of the catalyst by centrifugation, the concentration of MB was determined with a Perkin–Elmer Lambda 35 UV–vis spectrophotometer. The MB dye has an absorption maximum at 665 nm. The concentration of MB at diverse irradiation times was gained by converting absorbance of the solution to MB concentration (Beer–Lambert's law, $A = \varepsilon bC$, where A: absorption, ε: proportion constant, b: light length, C: concentration). A standard calibration curve (not shown here) was built by adjusting a different concentration of MB solution and the absorption at 665 nm. This calibration curve refers to the situation of the absence of byproducts co-adsorption. A blank test was done in the solution without a catalyst, where the concentration of the MB indicates constancy.

2.5. Photodegradation kinetics

Photocatalytic degradation of MB yields carbon dioxide, nitrate, sulfate, and water. The reaction can be written as follows [34]:

$$C_{16}H_{18}N_3S^+ + 25.5O_2 \longrightarrow 16CO_2 + 3NO_3^- + SO_2^- + 6H^+ + 6H_2O$$

If the reaction follows zero-order kinetics, is as shown in Eq. (1):

$$[MB]_i - [MB]_t = k_0 t \quad (1)$$

If the reaction follows first-order kinetics, is as shown in Eq. (2):

$$\ln \frac{[MB]_t}{[MB]_i} = -k_1 t \quad (2)$$

where $[MB]_i$ and $[MB]_t$ indicate MB concentration at $t = 0$ and $t = t$, respectively. If the reaction follows second-order kinetics, gives Eq. (3) which can also be rewritten in a non-linear form as shown in Eq. (4):

$$\frac{1}{[MB]_t} - \frac{1}{[MB]_e} = k_2 t \quad (3)$$

$$[MB]_t = \frac{[MB]_e}{[MB]_e k_2 t + 1} \quad (4)$$

3. Results and discussion

3.1. Textural characterization

Nitrogen physisorption is the method of choice to gain knowledge about nanoporous materials. This method gives information on the specific surface area and the pore diameter. Calculating pore diameters of nanoporous materials using the BJH method is common. Previous studies show that the application of the BJH theory gives appropriate qualitative results which allow a direct comparison of relative changes between different nanoporous materials [30].

Nitrogen adsorption isotherms of the MAC and Fe-MACs are shown in Fig. 1. A high adsorption at a low relative pressure reveals that MACs is mainly microporous. The increase in the adsorption at a high relative pressure is due to multilayer adsorption on the mesoporous, macroporous, and on the external surface [31]. The presence of hysteresis loop could be due to the existence of mesoporous. Table 1 shows the textural properties of the nanostructured samples as indicated by the N_2 adsorption isotherms. The iron oxide-supported MAC samples manifested a decreasing specific surface area as well as decreasing total and micropore volumes with increasing electroplating time. The pore size distributions (see the insets of Fig. 1) are slightly shifted to smaller values in contrast to the host materials. This effect is due to the mesopore filling with the iron oxide. Beside the reduction in the pore sizes, a slight broadening of the distributions is observed for the host–guest compounds.

In order to check the structural degradation, XRD data of carbonaceous adsorbents were obtained on Philips 1830 diffractometer using Cu Kα radiation of wavelength 0.154 nm. In Fig. 2, the XRD patterns of

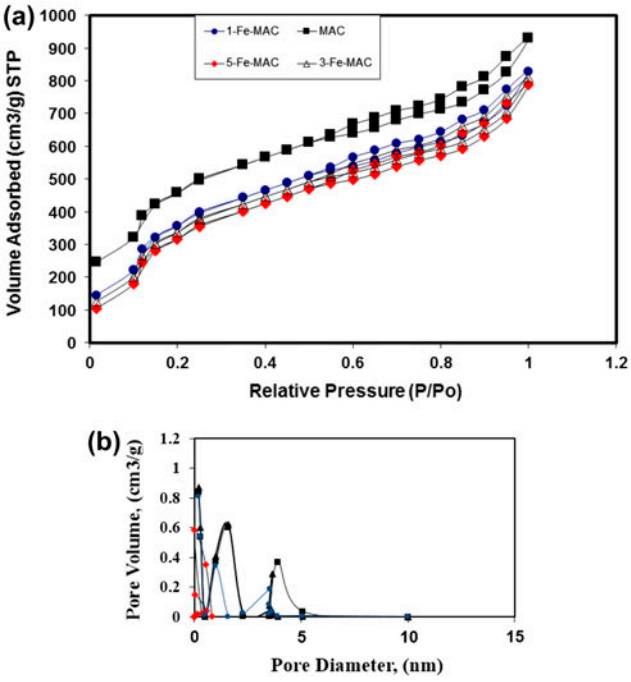

Fig. 1. (a) Adsorption–desorption isotherms of nitrogen at 77 K on MAC, 1-Fe-MAC, 3-Fe-MAC, and 5-Fe-MAC and (b) the BJH pore size distribution calculated from the desorption branch of the isotherm.

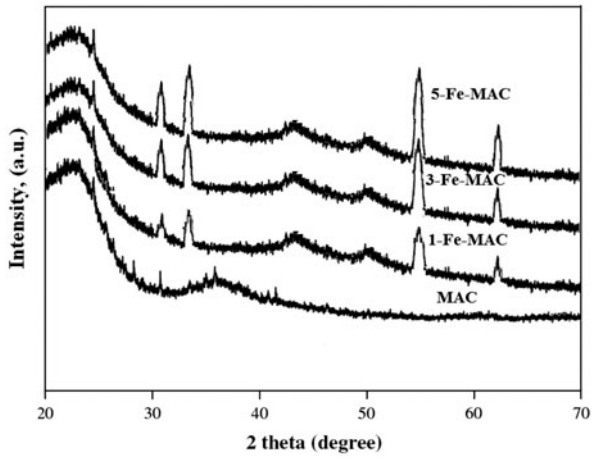

Fig. 2. Wide-angle XRD patterns of the microsporous activated carbon adsorbents (MAC, 1-Fe-MAC, 3-Fe-MAC, and 5-Fe-MAC).

MAC, 1-Fe-MAC, 3-Fe-MAC, and 5-Fe-MAC are presented. Well-defined peaks at 30.1˚, 35.4˚, 57˚, and 62.5˚ 2θ, characteristic of Fe_3O_4 appears after iron oxide modification. The strong and sharp peaks (especially in the case of 3-Fe-MAC and 5-Fe-MAC) indicate that large iron crystals formed outside of the carbon particles.

In order to understand the surface morphology, shape and size of iron oxide microporous activated carbon, SEM analysis was performed on 3-Fe-MAC sample (Fig. 3). SEM picture exhibits an irregular porous structure. The micrograph also revealed clearly that the resulting particles were almost perfectly loaded on carbonaceous surface.

Fig. 4 shows thermogravimetric analysis (TGA) curve of the 3-Fe-MAC using a heating rate of 5 ℃ min^{-1}. The 3-Fe-MAC composite showed a 78% weight loss from 360 to 520℃ related to the oxidation of the carbon. A weight of 22% is found after oxidation of the activated carbon, which is related to the Fe oxide in the prepared nanocomposite.

3.2. Photocatalytic activity of metal oxide-supported activated carbon photocatalyst

Fig. 5 displays the effectiveness of photocatalysts (iron oxide nanoparticles, MAC, 1-Fe-MAC, 3-Fe-MAC, and 5-Fe-MAC) in MB photodegradation in UV light. Among all photocatalysts, 3-Fe-MAC has been shown the best results for MB photodegradation. After 40 min irradiation, about 50% MB concentration was misplaced and after 75 min MB removed completely from media. The higher activity of 3-Fe-MAC was due to the presence of nanostructure carbon structure and iron oxide in optimum concentration. Several investigations have shown that carbon nanomaterials are good adsorbents for dye adsorption [34,35]. The experimental results have shown that the photodegradation activity of 3-Fe-MAC catalyst was clearly enhanced in contrast with the other

Table 1
Textural parameters of the MAC, 1-Fe-MAC, 3-Fe-MAC, and 5-Fe-MAC employed in this study

Adsorbent	Average pore diameter (nm)	A_{BET} (m^2 g^{-1})	Total pore volume (cm^3 g^{-1})	Micropore volume (cm^3 g^{-1})
MAC	2.3	1,640	0.93	0.73
1-Fe-MAC	2.2	1,547	0.88	0.72
3-Fe-MAC	2.22	1,531	0.86	0.69
5-Fe-MAC	2.21	1,511	0.81	0.64

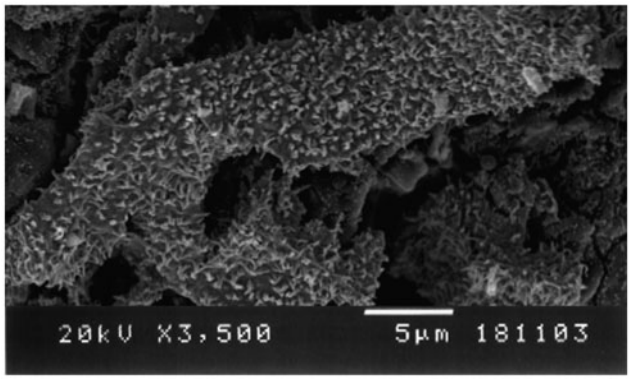

Fig. 3. SEM image of the 3-Fe-MAC.

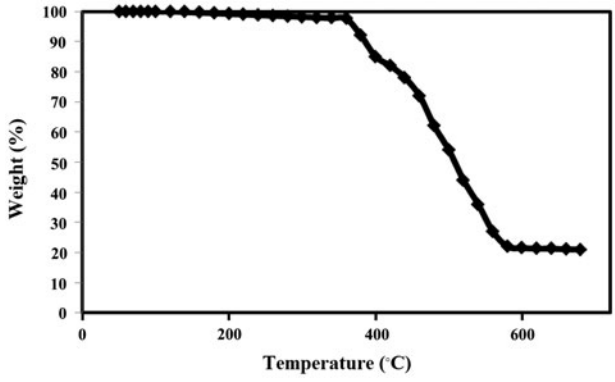

Fig. 4. TGA plot of the 3-Fe-MAC.

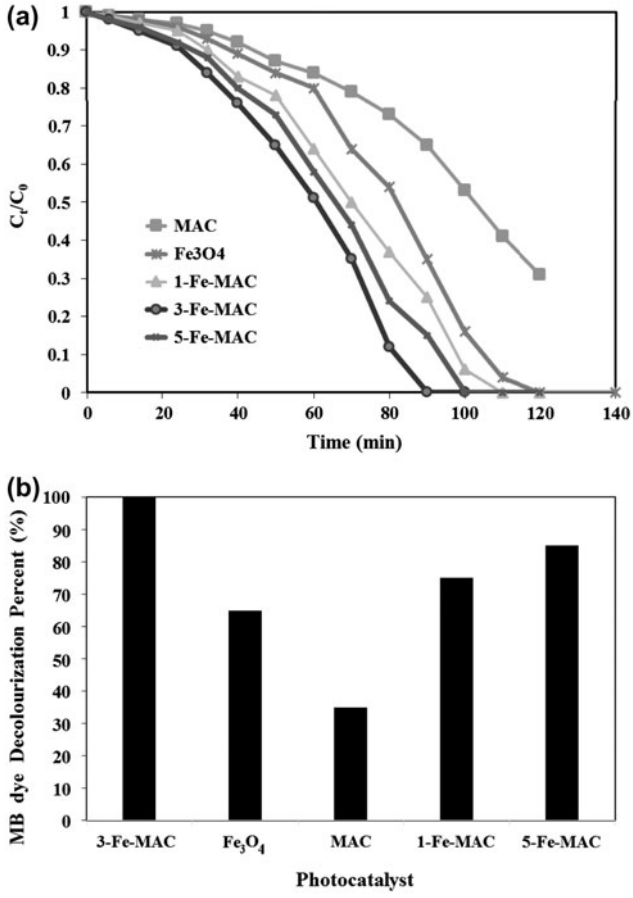

Fig. 5. The photocatalytic activities of Fe_3O_4, MAC, 1-Fe-MAC, 3-Fe-MAC, and 5-Fe-MAC photocatalysts (a) the effect of contact time (b) photocatalyst comparison in MB dye decolorization percent in tubular form at 90 min (catalyst dosage = 0.2 g/L, [MB] = 60 ppm, pH 4, temperature = 25°C).

photocatalysts. The iron oxide-supported activated carbon catalysts were more active than iron oxide nanoparticle (Fig. 5), probably due to the better porosity and structure. These outcomes propose that the loading of the iron oxide particles on the surface of the support and the better accessibility of the reactants might be more favorable for the photocatalytic reaction. The activated carbon had a larger specific surface area than iron oxide nanoparticles and iron oxide-modified activated carbon but had a lower catalytic activity.

The role of activated carbon structure in the enhancement of MB degradation by iron oxide might be because of

(1) Increasing adsorption capacity of the photocatalyst. MB molecules would transfer from the solution to the catalysts' surface and be adsorbed with offset face-to-face orientation via p–p conjugation between MB and aromatic regions of the carbonaceous photocatalyst. Therefore, the adsorption of dyes is increased compared to iron oxide.
(2) Extending light absorption. The chemical bonds of Fe–O–C and good transparency of carbonaceous photocatalyst made a red shift in the photo-responding range and facilitate a more efficient use of light for the photocatalysis.
(3) Overpowering charge recombination. Carbon surface can act as an acceptor of the photogenerated electrons for iron dioxide particles and confirm a fast charge moving in view of its great conductivity, and therefore, an effective charge separation can be attained [22]. The better charge transportation would provide more photo-induced carriers for the associated photocatalytic reactions, cause to a higher photocatalytic activity.

For kinetic estimation, the standard zero-, first-, and second-order kinetics equations were fitted to the

experimental data to conclude the appropriate model which shown the kinetic of degradation. Table 2 summarizes the fitting of the photodegradation data with various kinetics models. Based on linear regression method, the kinetic data of 3-Fe-MAC fits better to first-order model ($R^2 = 0.995$) and good degree of deviation (SSE = 11.09) than zero- and second-order models.

The photodegradation of MB dyes by 3-Fe-MAC under UV irradiation followed photocatalytic mechanism. Firstly, MB dye adsorbed on the surface of 3-Fe-MAC photocatalyst. In second step, MB dye molecule will photodegradated by UV irradiation. The photodegradation of MB dye is the rate-determining step which involves direct charge transfer from the 3-Fe-MAC to MB dye adsorbed at 3-Fe-MAC active surface. Finally, photon-generated holes (h^+_{vb}), electrons (e^-_{cb}), hydroxyl radicals ($OH^{\cdot}$), and superoxide ions ($O^{\cdot-}_2$) take part in redox reactions if thermodynamically promising [36,37]. The species h^+_{vb}, e^-_{cb}, ($OH^{\cdot}$), and ($O^{\cdot-}_2$) broke down MB dye molecule to small fragments that in the end decomposed into simple inorganic minerals. The photodegradation of MB by 3-Fe-MAC included the following reactions.

$$\text{Fe-MAC} \xrightarrow{hv} \text{Fe-MAC}\ (h^+ + e^-) \quad (5)$$

$$h^+ + OH^- \rightarrow OH^{\cdot} \quad (6)$$

$$O_2 + e^- \rightarrow O^{\cdot-}_2 \quad (7)$$

$$O^{\cdot-}_2 + e^- + 2H^+ \rightarrow H_2O_2 \quad (8)$$

$$O^{\cdot-}_2 + O^{\cdot-}_2 + 2H^+ \rightarrow H_2O_2 + O_2 \quad (9)$$

$$\text{MB dye} \xrightarrow{hv} \text{MB dye}^{\cdot} \quad (10)$$

$$\text{MB dye}^{\cdot} + \text{Fe-MAC} \rightarrow \text{MB dye}^{\cdot+} + \text{Fe-MAC}\ (e) \quad (11)$$

$$\text{MB dye}^{\cdot+} + O^{\cdot-}_2 \rightarrow CO_2 + H_2O \quad (12)$$

The effect of photocatalyst dosage on the photodegradation of MB was examined in UV irradiation by different dosage of 3-Fe-MAC varying from 0.02 to 0.2 g/L at a fixed dye concentration of 100 ppm. The photodegradation rate for photocatalyst is presented in Fig. 6, which shows that initial slopes of the curves rise greatly by increasing catalyst amount from 0.01 to 0.15 g/L and after that the amount of degradation remains almost constant. Hence, the maximum photodegradation is shown with 0.15 g/L dose of 3-Fe-MAC. The MB dye degradation improved meaningfully by increasing the dosage of photocatalyst. The increase in the amount of catalyst increases the number of active sites of iron oxide that in turn growths the number of $OH^{\cdot}$ and $O^{\cdot-}_2$ radicals. The photocatalytic destruction of other organic pollutants has also shown a similar type of dependence on photocatalyst dosage [38–40].

The influence of dye concentration on photodegradation was investigated by changing the MB concentration from 50 to 150 ppm at a 0.15 g/L of 3-Fe-MAC. Fig. 7 displays the rate of photodegradation in different concentrations of dye. It is observed from Fig. 7 that photodegradation speed decreases from 50 to 100 ppm and then it becomes almost constant up to 150 ppm.

Fig. 7 shows a high efficiency at low initial concentration of dye (50 ppm), which decreased with the increase in substrate concentration from 50 to 100 ppm and then it became almost constant. Increasing the dye concentration from 100 to 150 ppm decreased the degradation efficiency from 99.6 to 21.5%. Similar results were obtained earlier by other researches [41]. It is due to the fact that with the rise in initial concentration of dye, in the presence of UV irradiation and catalyst dose constant, more dye molecules are adsorbed onto the surface of activated carbon.

The photocatalytic degradation of MB has been investigated in the pH range of 2–10 at a fixed MB concentration of 100 ppm and 3-Fe-MAC dosage (0.15 g/L). The consequences are shown in Fig. 8. It is perceived that the degradation rises in the neutral to high pH range as compared to the acidic pH situations. Implementation of the reaction rate in basic

Table 2
Zero-, first-, and second-order kinetics data of photocatalytic kinetics of MB degradation on 3-Fe-MAC photocatalyst

	Zero-order			First-order			Second-order		
Sample	k_0	R^2	SSE	$k_1 \times 10^{-3}$	R^2	SSE	$k_2 \times 10^{-4}$	R^2	SSE
3-Fe-OMC	1.012	0.984	21.06	9.904	0.995	11.09	1.43	0.991	16.41

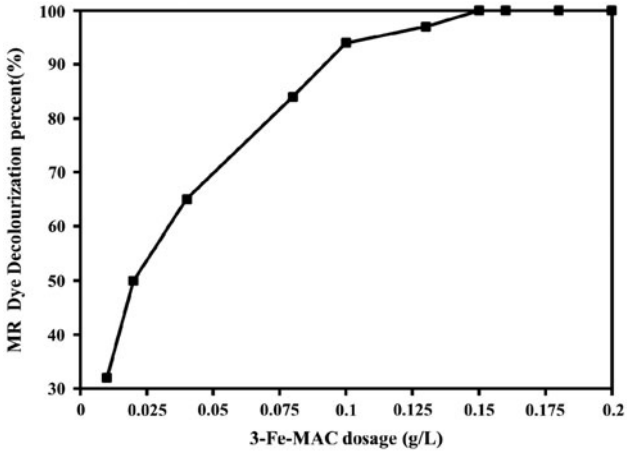

Fig. 6. The influence of 3-Fe-MAC amount on the degradation of MB dye ([MB dye] = 100 ppm, reaction time = 3 h, pH 6.5, temperature = 25˚C).

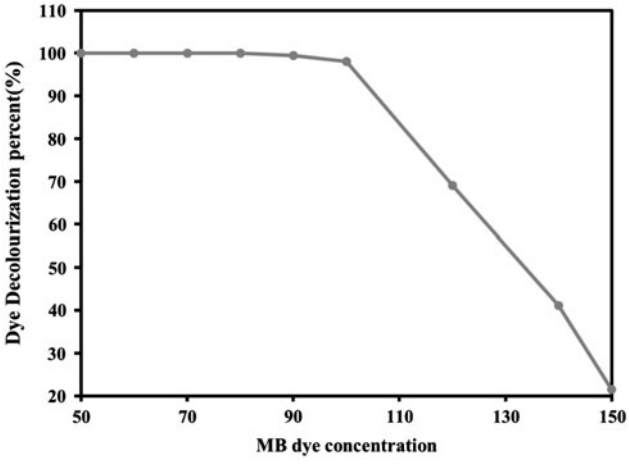

Fig. 7. The influence of MB dye concentration on the degradation of MB on 3-Fe-MAC (3-Fe-MAC dosage = 0.15 g/L, reaction time = 3 h, pH 4, temperature = 25˚C).

environments might be credited to the growth of hydroxyl ions, which in turn prompts the formation of more hydroxyl radical formation.

4. Conclusions

Carbon nanoporous photocatalyst was synthesized using a low-cost carbon source after that modified with iron oxide. The structural order and textural properties of the modified and unmodified activated photocatalysts were studied by XRD and nitrogen adsorption analyses. The photocatalytic activity of the iron oxide nanoparticles, activated carbon, and iron

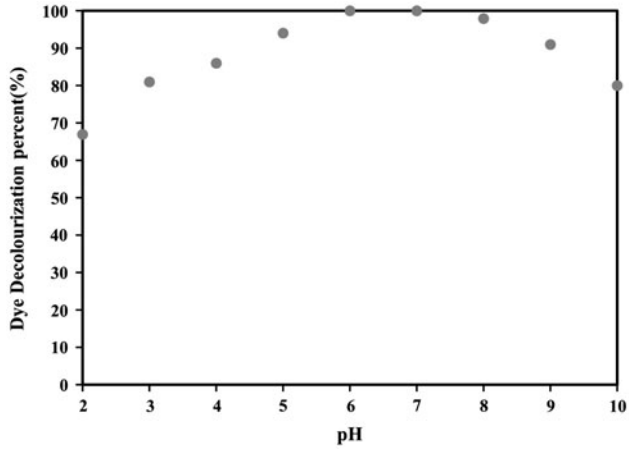

Fig. 8. The influence of pH on the degradation of MB dye on 3-Fe-MAC photocatalyst ([MB dye] = 100 ppm, 3-Fe-MAC dosage = 0.15 g/L, reaction time = 3 h, temperature = 25˚C).

oxide-modified activated carbon composites (1-Fe-MAC, 3-Fe-MAC and 5-Fe-MAC) was examined by the degradation of MB in aqueous solutions under UV light irradiation. It was observed that the pH, concentration of MB dye, and photocatalyst dosage significantly affect the decolorization of the dye. The degradation efficiency of MB dye with the iron oxide-modified activated carbons was much higher than that with pristine activated carbon and iron oxide nanoparticles. The enhancement of MB degradation by iron oxide is mainly because of (a) increasing adsorption capacity of the photocatalyst, (b) extending light absorption, and (c) overpowering charge recombination in iron oxide-modified activated carbon. Thus, iron oxide-modified activated carbon could be used as a practical and useful photocatalyst for the removal of dyes from wastewater which contributes to the environmental pollution.

Acknowledgments

The authors thank The Research Council at the Azad University for financial support.

References

[1] K. Ravikumar, B. Deebika, K. Balu, Decolourization of aqueous dye solutions by a novel adsorbent: Application of statistical designs and surface plots for the optimization and regression analysis, J. Hazard. Mater. 122 (2005) 75–83.
[2] J.W. Lee, S.P. Choi, R. Thiruvenkatachari, W.G. Shim, H. Moon, Evaluation of the performance of adsorption and coagulation processes for the maximum removal of reactive dyes, Dyes Pigm. 69 (2006) 196–203.

[3] J.R. Easton, P. Cooper, Colour in Dyehouse Effluent, the Society of Dyers and Colorists, Alden, Oxford, 1995, pp. 9–21.
[4] P.K. Dutta, An overview of textile pollution and its remedy, Indian J. Environ. Prot. 14 (1994) 443–446.
[5] K.C. Chen, J.Y. Wu, C.C. Huang, Y.M. Liang, S.C.J. Hwang, Decolorization of azo dye using PVA-immobilized microorganisms, J. Biotechnol. 101 (2003) 241–252.
[6] R. Gong, Y. Ding, M. Li, C. Yang, H. Liu, Y. Sun, Utilization of powdered peanut hull as biosorbent for removal of anionic dyes from aqueous solution, Dyes Pigm. 64 (2005) 187–192.
[7] I.A. Tan, A.L.W. Ahmad, B.H. Hameed, Adsorption of basic dye on high-surface-area activated carbon prepared from coconut husk: Equilibrium, kinetic and thermodynamic studies, J. Hazard. Mater. 154 (2008) 337–346.
[8] V.K. Gupta, A. Suhas, I. Ali, Removal of rhodamine B, fast green, and methylene blue from wastewater using red mud, an aluminum industry waste, Ind. Eng. Chem. Res. 43 (2004) 1740–1747.
[9] V.K. Gupta, S.K. Srivastava, D. Mohan, S. Sharma, Design parameters for fixed bed reactors of activated carbon developed from fertilizer waste for the removal of some heavy metal ions, Waste Manage. 17 (1997) 517–522.
[10] V.K. Gupta, S. Agarwal, T.A. Saleh, Synthesis and characterization of alumina-coated carbon nanotubes and their application for lead removal, J. Hazard. Mater. 185 (2011) 17–23.
[11] V.K. Gupta, A. Nayak, Cadmium removal and recovery from aqueous solutions by novel adsorbents prepared from orange peel and Fe_2O_3 nanoparticles, Chem. Eng. J. 180 (2012) 81–90.
[12] V.K. Gupta, I. Ali, T.A. Saleh, A. Nayak, S. Agarwal, Chemical treatment technologies for waste-water recycling—An overview, RSC Adv. 2 (2012) 6380–6388.
[13] A. Mittal, J. Mittal, A. Malviya, V.K. Gupta, Adsorptive removal of hazardous anionic dye "Congo red" from wastewater using waste materials and recovery by desorption, J. Colloid Interface Sci. 340 (2009) 16–26.
[14] A.K. Jain, V.K. Gupta, A. Bhatnagar, A comparative study of adsorbents prepared from industrial wastes for removal of dyes, Sep. Sci. Technol. 38 (2003) 463–481.
[15] A. Mittal, D. Kaur, A. Malviya, J. Mittal, V.K. Gupta, Adsorption studies on the removal of coloring agent phenol red from wastewater using waste materials as adsorbents, J. Colloid Interface Sci. 337 (2009) 345–354.
[16] A. Mittal, J. Mittal, A. Malviya, V.K. Gupta, Removal and recovery of chrysoidine Y from aqueous solutions by waste materials, J. Colloid Interface Sci. 344 (2010) 497–507.
[17] A. Mittal, J. Mittal, A. Malviya, D. Kaur, V.K. Gupta, Decoloration treatment of a hazardous triarylmethane dye, light green SF (Yellowish) by waste material adsorbents, J. Colloid Interface Sci. 342 (2010) 518–527.
[18] T.A. Saleh, V.K. Gupta, Column with CNT/magnesium oxide composite for lead(II) removal from water, Environ Sci. Pollut. Res. 19 (2012) 1224–1228.
[19] V.K. Gupta, R. Jain, A. Mittal, T.A. Saleh, A. Nayak, S. Agarwal, S. Sikarwar, Photo-catalytic degradation of toxic dye amaranth on TiO_2/UV in aqueous suspensions, Mater. Sci. Eng., C 32 (2012) 12–17.
[20] V.K. Gupta, R. Jain, A. Nayak, S. Agarwal, M. Shrivastava, Removal of the hazardous dye-Tartrazine by photodegradation on titanium dioxide surface, Mater. Sci. Eng., C 31 (2011) 1062–1067.
[21] S. Karthikeyan, V.K. Gupta, R. Boopathy, A. Titus, G. Sekaran, A new approach for the degradation of high concentration of aromatic amine by heterocatalytic Fenton oxidation: Kinetic and spectroscopic studies, J. Mol. Liq. 173 (2012) 153–163.
[22] T.A. Saleh, V.K. Gupta, Photo-catalyzed degradation of hazardous dye methyl orange by use of a composite catalyst consisting of multi-walled carbon nanotubes and titanium dioxide, J. Colloid Interface Sci. 371 (2012) 101–106.
[23] A. Fujishima, K. Honda, Electrochemical photolysis of water at a semiconductor electrode, Nature 238 (1972) 37–38.
[24] B. O'Regan, M. Grätzel, A low-cost, high-efficiency solar cell based on dye-sensitized colloidal TiO_2 films, Nature 353 (1991) 737–740.
[25] Z. Wang, W. Cai, X. Hong, X. Zhao, F. Xu, C. Cai, Photocatalytic degradation of phenol in aqueous nitrogen-doped TiO_2 suspensions with various light sources, Appl. Catal., B 57 (2005) 223–231.
[26] H. Khani, M.K. Rofouei, P. Arab, V.K. Gupta, Z. Vafaei, Multi-walled carbon nanotubes-ionic liquid-carbon paste electrode as a super selectivity sensor: Application to potentiometric monitoring of mercury ion(II), J. Hazard. Mater. 183 (2010) 402–409.
[27] S.H. Kim, H.H. Ngo, H.K. Shon, S. Vigneswaran, Adsorption and photocatalysis kinetics of herbicide onto titanium oxide and powdered activated carbon, Sep. Purif. Technol. 58 (2008) 335–342.
[28] D. Liu, J. Lei, L. Guo, K. Deng, A nanoparticle assembly method for the production of crystalline ordered mesoporous titanium oxide/carbon composites, Micropor. Mesopor. Mater. 139 (2011) 87–93.
[29] S.H. Joo, S.J. Choi, I. Oh, J. Kwak, Z. Liu, O. Terasaki, R. Ryoo, Ordered nanoporous arrays of carbon supporting high dispersions of platinum nanoparticles, Nature 412 (2001) 169–172.
[30] S.E. Moradi, Low-cost metal oxide activated carbon prepared and modified by microwave heating method for hydrogen storage, Korean J. Chem. Eng. 31 (2014) 1651–1655.
[31] M. Hejazifar, S. Azizian, H. Sarikhani, Q. Li, D. Zhao, Microwave assisted preparation of efficient activated carbon from grapevine rhytidome for the removal of methyl violet from aqueous solution, J. Anal. Appl. Pyrolysis 92 (2011) 258–266.
[32] U. Ciesla, F. Schüth, Ordered mesoporous materials, Micropor. Mesopor. Mater. 27 (1999) 131–149.
[33] D. Dollimore, G.R. Heal, Pore-size distribution in typical adsorbent systems, J. Colloid Interface Sci. 33 (1970) 508–519.
[34] S. Brunauer, P.H. Emmett, E. Teller, Adsorption of gases in multimolecular layers, J. Am. Chem. Soc. 60 (1938) 309–319.
[35] R. Prakash, K. Fanselau, S. Ren, T.K. Kumar Mandal, C. Kübel, H. Hahn, M. Fichtner, A facile synthesis of a carbon-encapsulated Fe_3O_4 nanocomposite and its

performance as anode in lithium-ion batteries, Beilstein J. Nanotechnol. 4 (2013) 699–704.
[36] A. Houas, H. Lachheb, M. Ksibi, E. Elaloui, C. Guillard, J.M. Herrmann, Photocatalytic degradation pathway of methylene blue in water, Appl. Catal., B 31 (2001) 145–157.
[37] M.M. Haque, M. Muneer, Photodegradation of norfloxacin in aqueous suspensions of titanium dioxide, J. Hazard. Mater. 145 (2007) 51–57.
[38] M. Muruganandham, M. Swaminathan, Photocatalytic decolouration and degradation of reactive orange 4 by iron oxide-uv process, Dyes Pigm. 76 (2006) 113–117.
[39] A. Akyol, H.C. Yatmaz, M. Bayramoglu, Photocatalytic decolorization of Remazol Red RR in aqueous ZnO suspensions, Appl. Catal., B 54 (2004) 19–24.
[40] A.K. Jain, V.K. Gupta, A. Bhatnagar, S. Jain Suhas, A comparative assessment of adsorbents prepared from industrial wastes for the removal of cationic dye, J. Indian Chem. Soc. 80 (2003) 267–270.
[41] A.K. Subramani, K.S. Byrappa, S. Ananda, K.M. Lokanatha Rai, C. Ranganathaiah, M. Yoshimura, Photocatalytic degradation of indigo carmine dye using TiO_2 impregnated activated carbon, Bull. Mater. Sci. 30 (2007) 37–41.